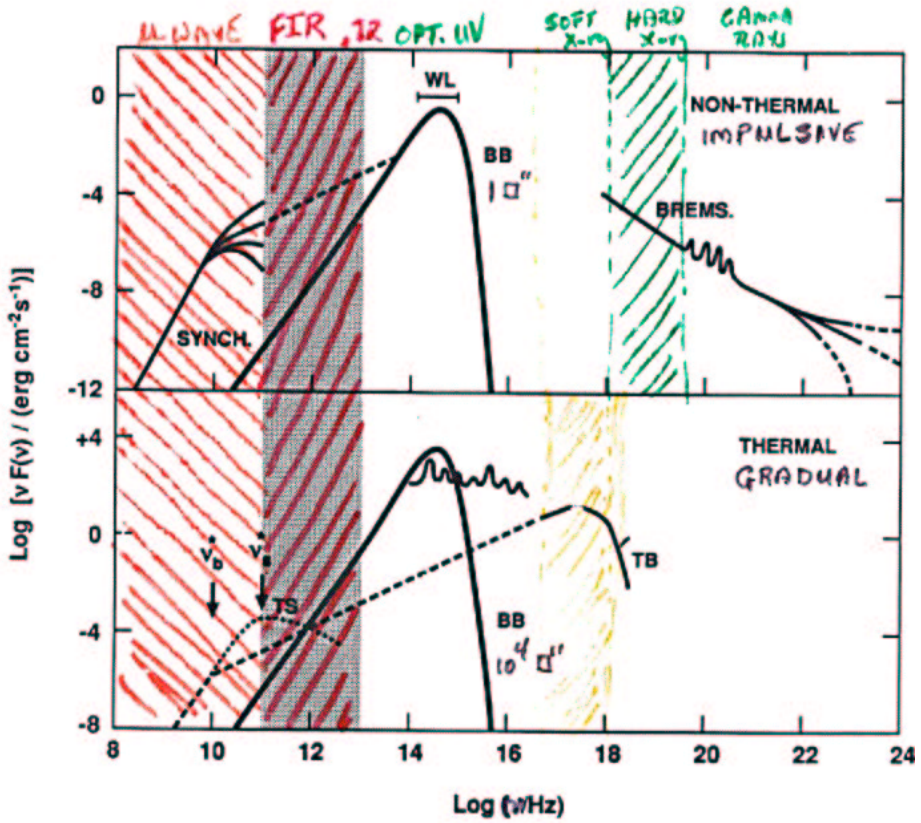

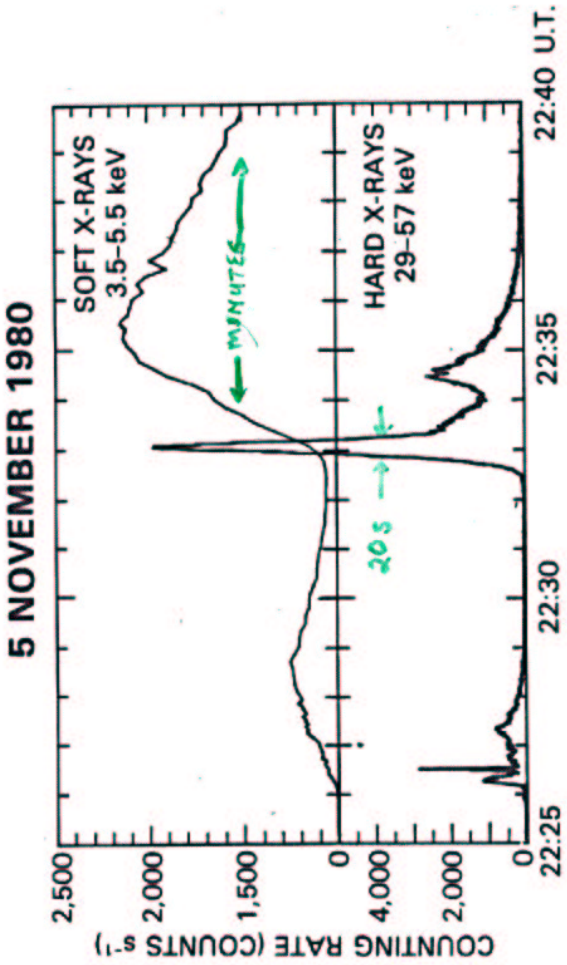

Figure 1: Soft and hard X-ray emissions as a function of time for the two flares on 1980 November 5. The soft X-ray counting rate is the sum of the counts in the HXIS band 1 in selected pixels of the coarse field of view. The hard X-ray rate is the sum of counts in HXRBS channels 1 and 2.

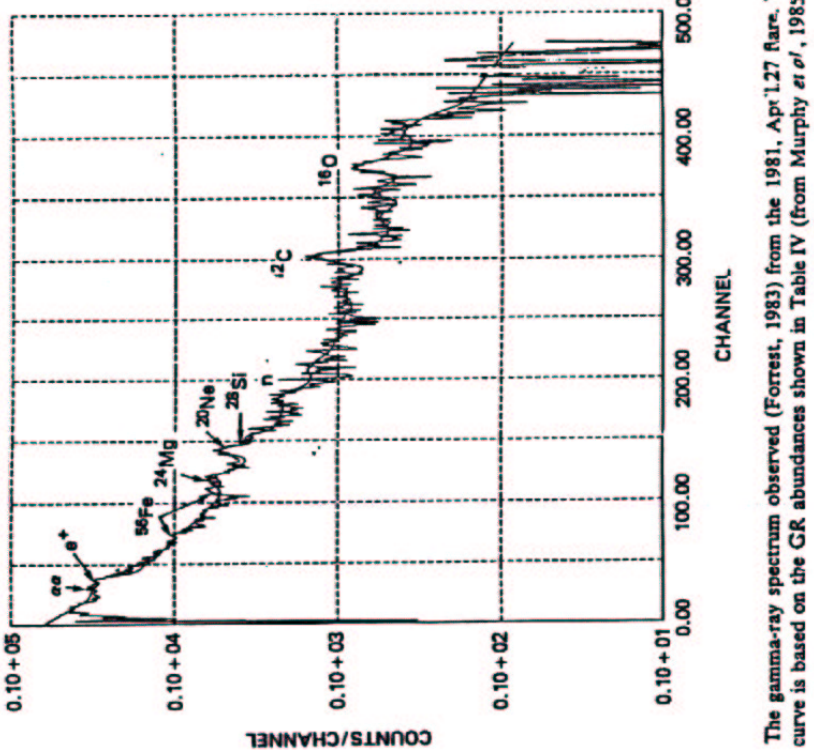

The gamma-ray spectrum observed (Forrest, 1983) from the 1981, April 27 flare. The smooth curve is based on the GR abundances shown in Table IV (from Murphy *et al*., 1985b).

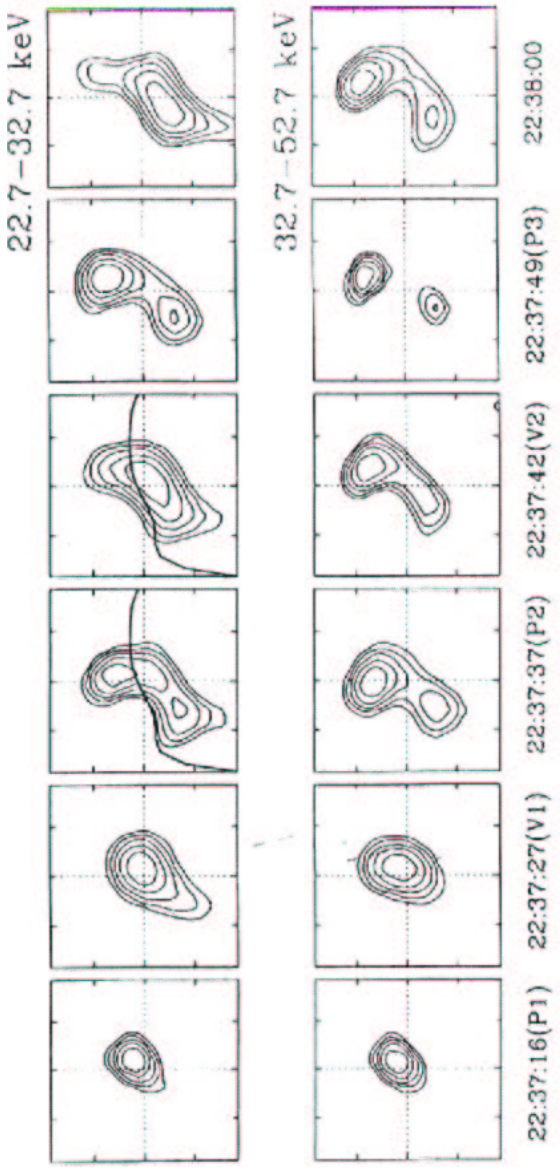

Figure 6.7

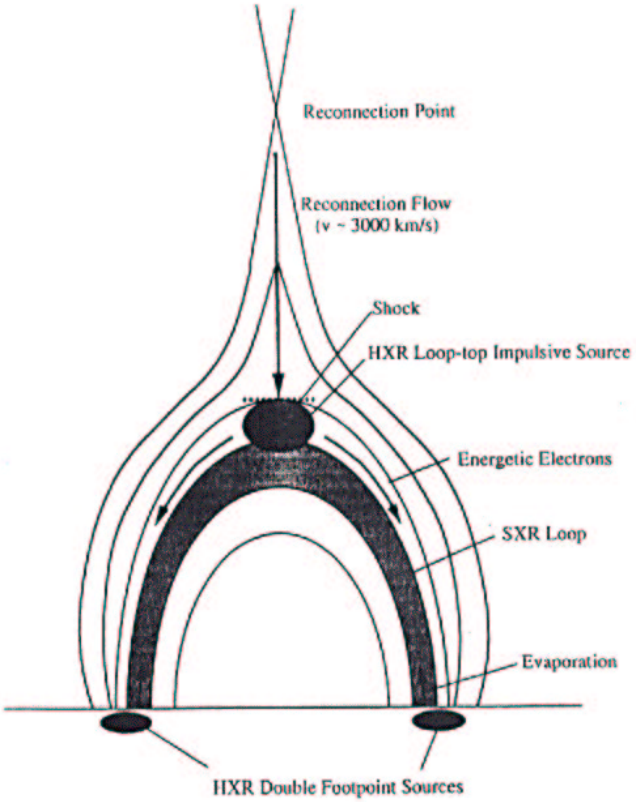

Figure 2.9

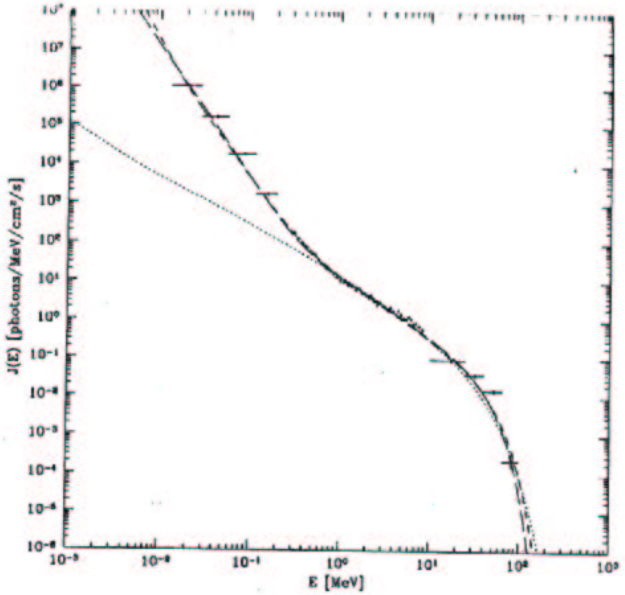

Fig. 4.— The GRS photon spectrum (cross hair) of the first 1989 March 6 impulsive burst (UT 13:57:29 – 13:58:34) compared to three models, hard sphere (short dashed line), whistler (medium dashed line), and the general (long dashed line). The fitted parameter are given in Table 1.

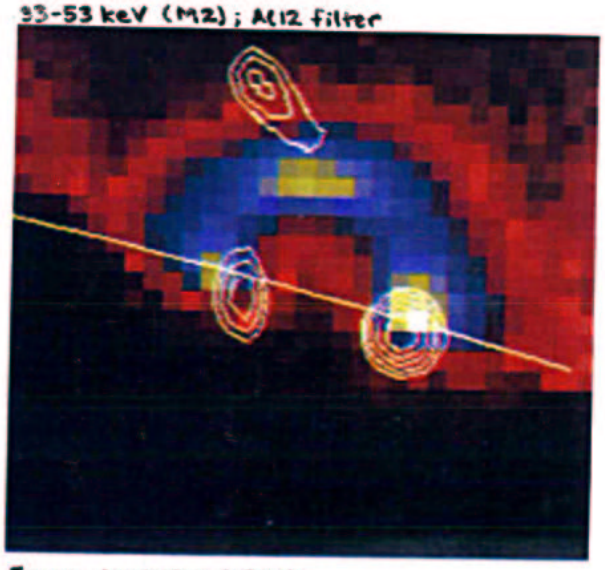

From MASUDA (1993)

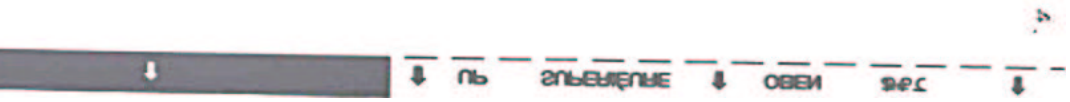

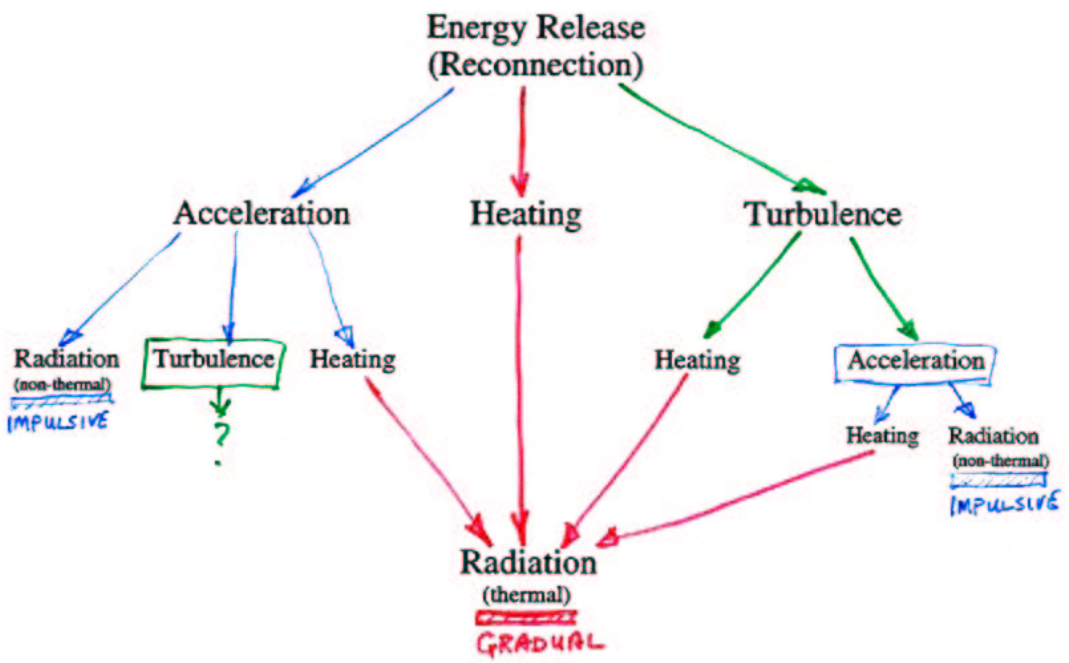

Acceleration
(Possible Mechanisms)

1) Electric Fields (parallel to B field)

Dricer Field $\mathcal{E}_D \simeq 10^{-5}$ V/cm

Energy Gain $\Delta E \simeq kT(L/\lambda_{coll}) \sim$ few keV $(\mathcal{E} \ll \mathcal{E}_D)$

$\mathcal{E} > \mathcal{E}_D$ RUNAWAY ELECTRONS, UNSTABLE $\Rightarrow$ TURBULENCE

2) Shocks (First Order Fermi)

Need Scattering (turbulence ?)

Efficient at High Energies

Rate Governed by Scattering ($\tau_{scat} \simeq D_{\mu\mu}^{-1}$)

ACCELERATION RATE $\sim \frac{U_{SHOCK}}{v} D_{\mu\mu}$

3) Stochastic (Turbulence, Waves)

(Second Order Fermi)

$\tau_{scat} \simeq D_{\mu\mu}^{-1}$, $\tau_{acc} \simeq p^2/D_{pp}$ $\left[\propto \Omega^{-1}(B^2/8\pi w_{waves})\right]$

At high energies, $\tau_{scat} << \tau_{acc}$, similar to shocks but slower by β

At low energies $\tau_{acc} \ll \tau_{scat}$ more efficient than shocks

Stochastic Acceleration Model

Fokker-Planck Equation

$$\frac{\partial f}{\partial t} = \frac{\partial^2}{\partial E^2}[D(E)f] - \frac{\partial}{\partial E}[(A(E) - |\dot{E}_L|)f] - \frac{f}{T_{esc}(E)} + Q(E)$$

where

$f(E,t)$ = # particles/volume

E = Kinetic Energy, in units of $m_e c^2$

$D(E)$ = Diffusion Rate

$A(E)$ = Systematic Acceleration Rate

$|\dot{E}_L|$ = non-stochastic loss rates

$T_{esc}(E)$ = particle escape time

$Q(E)$ = Source Term

Stochastic Acceleration Model

Loss Rates

$$|\dot{E}_L| = \dot{E}_{Coul} + \dot{E}_{Synch} = -4\pi r_0^2 cn \ln\Lambda/\beta - 4\alpha r_0^2 B^2\beta^2\gamma^2/9m_e c^2$$
$$= 6\times 10^{-2} s^{-1}\left(\frac{n}{10^{11}\ cm^{-3}}\right)\frac{1}{\beta} + 3.3\times 10^{-4} s^{-1}\left(\frac{B}{500\ G}\right)^2\beta^2\gamma^2$$

Source Term

$$Q(E) = Q_0\frac{2}{\sqrt{\pi}}\sqrt{\frac{E}{kT}}\exp\left(-\frac{E}{kT}\right)$$

$$kT = 1.5 \text{ keV}$$

Definition of Coefficients (General Form)

$$D(E) = \mathcal{D}\beta(\gamma\beta)^q$$

$$A(E) = \mathcal{D}(q+2)(\gamma\beta)^{q-1}$$

$$T_{esc}(E) = \mathcal{T}_{esc}(\gamma\beta)^s/\beta + \frac{L}{\beta c\sqrt{2}}$$

Stochastic Acceleration Model

Whistler Model

- Model Parameters related

$$\mathcal{D} = \frac{\pi(\tilde{q}-1)^2}{\tilde{q}^2(\tilde{q}-2)(\tilde{q}+2)}\left(\frac{ck_{min}}{\Omega_e}\right)^{\tilde{q}-1}\alpha^{-4}R\Omega_e$$

$$\frac{\mathcal{T}_{esc}}{\mathcal{D}} = \frac{\tilde{q}^2(\tilde{q}-2)}{(\tilde{q}-1)^2(\tilde{q}+1)}\alpha^4\left(\frac{L}{c}\right)^2$$

$$q = s = \tilde{q} - 2$$

$$\alpha = \frac{\omega_{p,e}}{\Omega_e} = 2.0\left(\frac{n}{10^{11}cm^{-3}}\right)^{1/2}\left(\frac{B}{500\ G}\right)^{-1}$$

General Model

- No relation between model parameters

Photon Production

Thin Target

$$J_{AS}(k) = L\int_k^\infty dE f_{AS}(E)\beta c n_{AS}\frac{d\sigma}{dk}(E,k)$$

Thick Target

$$f_{thick}(E) = -\frac{1}{\dot{E}_C}\int_E^\infty \frac{f_{AS}}{T_{esc}}dE$$

$$J_{FP}(k) = L\int_k^\infty dE f_{thick}\beta c n\frac{d\sigma}{dk}(E,k)$$

General Results

(with Petrosian ApJ 1997, 1998, 1999)

1. **High Energies** (Exact value depends on plasma parameters)

$D_{\mu\mu} \gg D_{pp}/p^2$

Isotropic, Diffusion Equation

$\alpha = \frac{\omega_p}{\Omega}\propto \frac{\sqrt{n}}{B}$

$\alpha = \sqrt{\frac{m_e}{m_p}}\frac{1}{\beta_A}$

2. **Low Energies** $D_{\mu\mu} \ll D_{pp}/p^2$

Pure (Anisotropic) Acceleration

3. For Acceleration of Background (Thermal) Particles Stochastic Acceleration More Efficient.

Shock Important For Higher Energy (Relativistic?) Particles

4. Pitch Angle Distribution Energy Dependent. Important For "Resolved" Sources

5. These Effects Are Important For Low α Plasmas

Weak dependence on turbulence spectrum

Thick - Target
Particle Spectrum

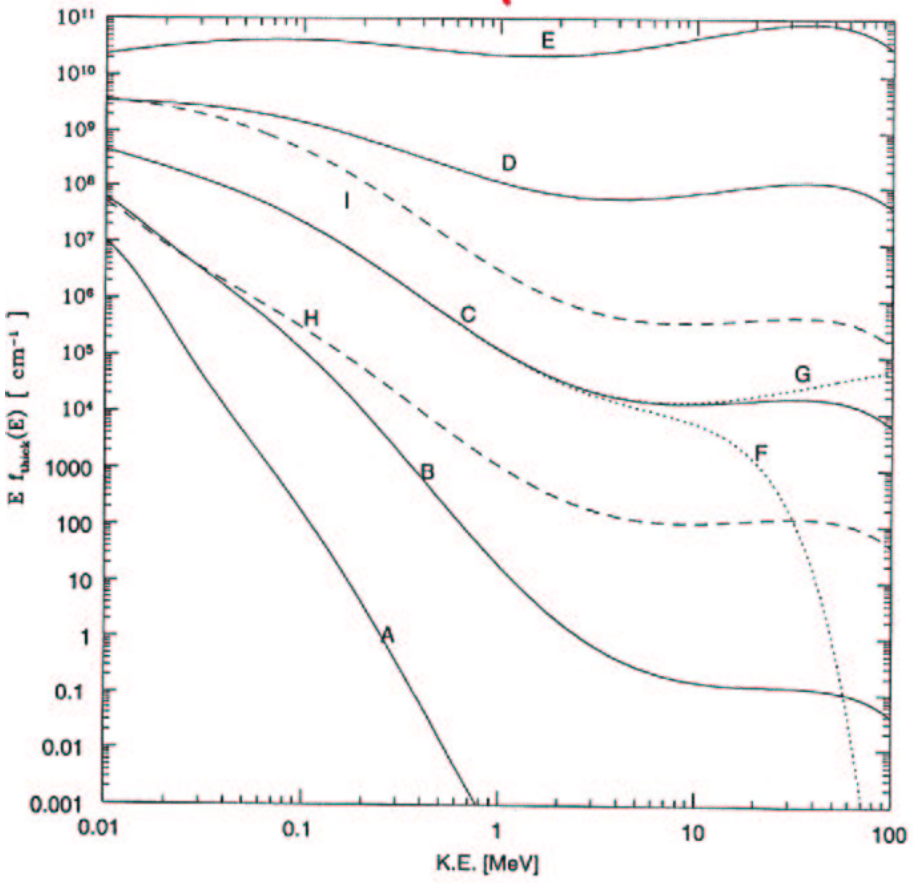

K.E. [MeV]

Foot - Point
Photon Spectrum

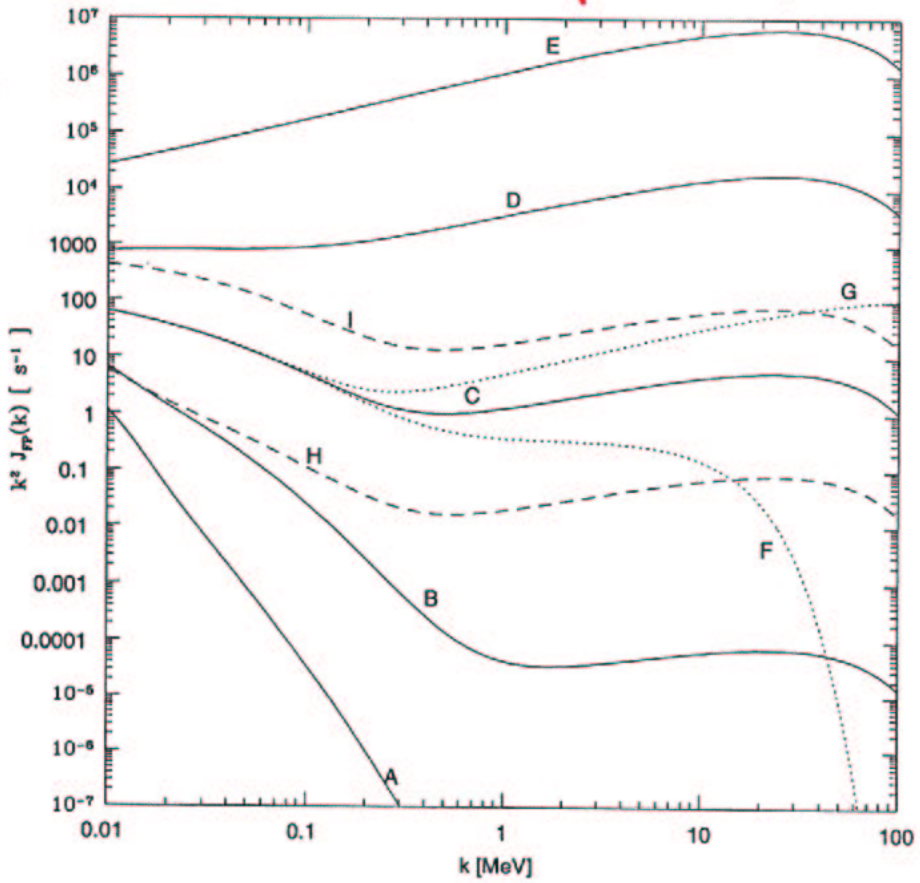

Loop - Top Photon Spectrum

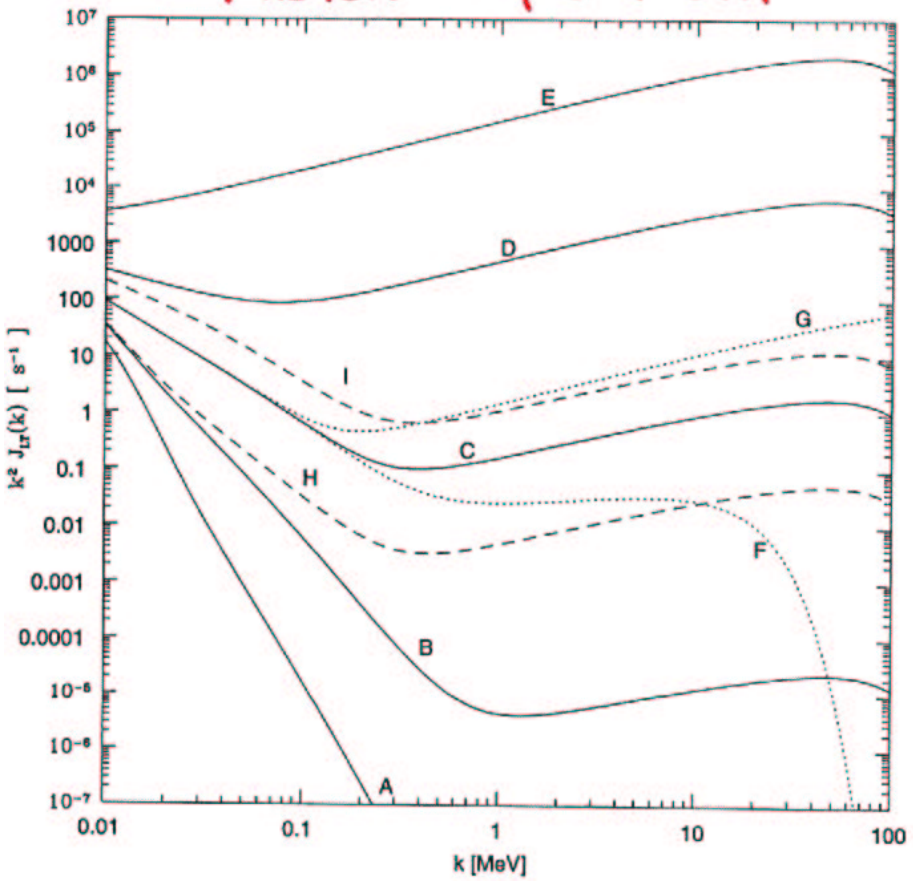

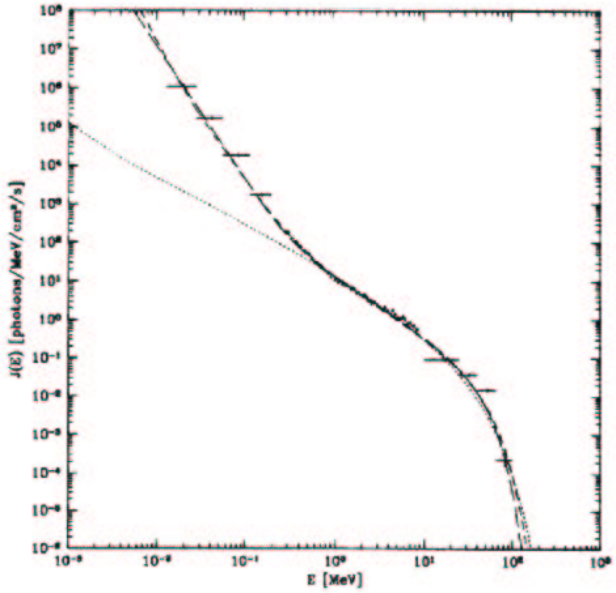

Fig. 4.— The GRS photon spectrum (cross hair) of the first 1989 March 6 impulsive burst (UT 13:57:29 – 13:58:34) compared to three models. hard sphere (short dashed line), whistler (medium dashed line), and the general (long dashed line). The fitted parameter are given in Table 1.

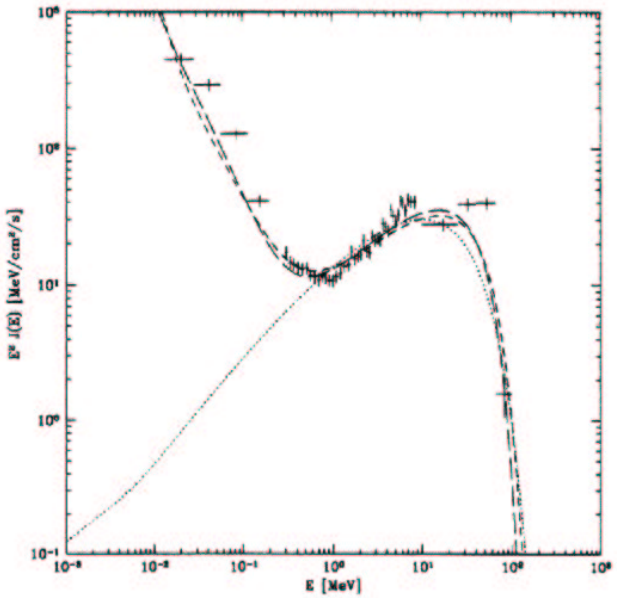

Fig. 5.— Same as Figure 4 except we plot the power $J(E)E^2$ instead of photon flux $J(E)$. Note that in this representation, the linear integral under the log-log graph is the amount of photon energy in that interval. This representation also magnifies the differences between the model fit and the data points.

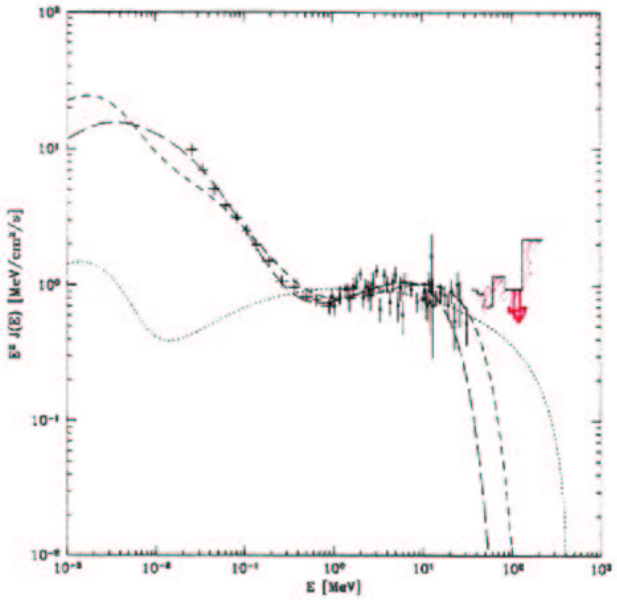

Fig. 7.— The BATSE (cross hair) and EGRET (solid bullet with vertical error bars) data of the 1991 June 30 flare (UT 2:55:32 - 2:57:11) compared to three models (same as Fig. 4). The solid histogram at high energy is the EGRET 2-σ upper limits. The EGRET data are identical to that given in Dingus et al. (1994) except that only every third data points are plotted between 1 and 10 MeV for clarity. The BATSE photon flux in each channel is inferred from the photon counts in each channel by comparing the ratio of the observed counts and the predicted model counts. The fitting is performed using the actual photon counts in each channel through the BATSE detector response matrix. The first and last energy channels were not used in the fitting procedure, and the fitted parameters of the models are given in Table 3.

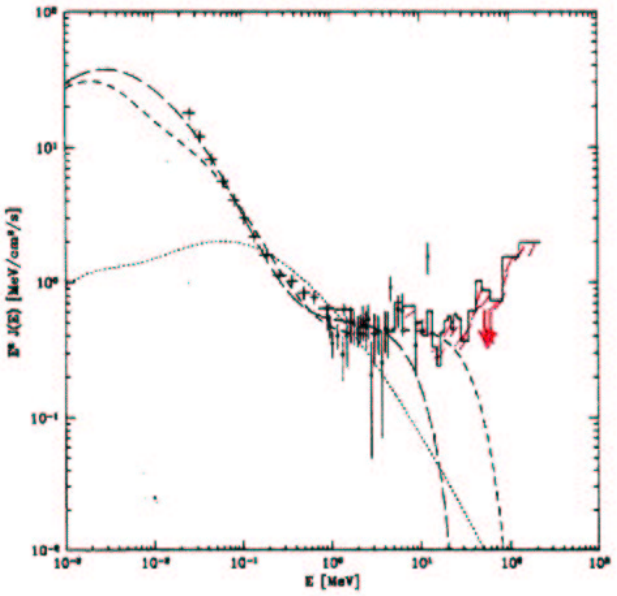

Fig. 8.— Same as Fig. 7 for the 1991 July 2 flare (UT 19:35:19 – 19:37:01). The fitted parameters of the models are given in Table 4.

parameters	hardsphere	whistler	general
$Q_0[\mathrm{cm}^{-3}\mathrm{s}^{-1}]$	$(1.4 \pm 0.1) \times 10^{8}$	$(1.7 \pm 0.1) \times 10^{13}$	$(7.7 \pm 5.1) \times 10^{12}$
$n[\mathrm{cm}^{-3}]$	$(7.5 \pm 0.1) \times 10^{10}$	$(2.9 \pm 0.1) \times 10^{11}$	$(1.62 \pm 0.43) \times 10^{11}$
B[G]	2007 ± 29	500 ± 40	325 ± 66
q	2	1.45 ± 0.02	1.22 ± 0.09
s	0	q	1.87 ± 0.14
T[s]	1.38 ± 0.03	0.12	$0.090 \pm .006$
L[cm]	10^{9}	$(2.8 \pm 0.41) \times 10^{9}$	10^{9}
R		7×10^{-5}	
ν	45	44	43
χ^2/ν	15	6.1	4.9

Table 1 Model parameters for the first impulsive peak of the 1989 March 6 flare.

parameters	hardsphere	whistler	general
$Q_0[\mathrm{cm}^{-3}\mathrm{s}^{-1}]$	$(3.4 \pm 0.7) \times 10^{8}$	$(1.7 \pm 1.0) \times 10^{9}$	$(2.7 \pm 0.1) \times 10^{9}$
$n[\mathrm{cm}^{-3}]$	$(5.4 \pm 0.5) \times 10^{11}$	$(3.6 \pm 0.3) \times 10^{11}$	$(1.9 \pm 0.1) \times 10^{11}$
B[G]	2400 ± 170	500 ± 20	825 ± 34
q	2	1.23 ± 0.02	1.32 ± 0.04
s	0	q	1.33 ± 0.03
T[s]	0.083 ± 0.001	0.03	0.022 ± 0.001
L[cm]	10^{9}	$(4.6 \pm 0.1) \times 10^{8}$	10^{9}
R		3×10^{-5}	
ν	25	24	23
χ^2/ν	5.1	2.6	2.3

Table 2 Model parameters for the second impulsive peak of the 1989 March 6 flare.

parameters	hardsphere	whistler	general
$Q_0[\mathrm{cm}^{-3}\mathrm{s}^{-1}]$	$(4.5 \pm 0.5) \times 10^{9}$	$(1.9 \pm 0.2) \times 10^{10}$	$(1.51 \pm 0.03) \times 10^{10}$
$n[\mathrm{cm}^{-3}]$	$(1.11 \pm 0.01) \times 10^{11}$	$(1.95 \pm 0.01) \times 10^{11}$	$(4.4 \pm 0.2) \times 10^{10}$
B[G]	93 ± 16	392 ± 20	644 ± 15
q	2	1.33 ± 0.01	1.34 ± 0.01
s	0	q	1.71 ± 0.02
T[s]	0.49 ± 0.01	0.15	0.096 ± 0.001
L[cm]	10^{9}	$(2.92 \pm 0.02) \times 10^{9}$	10^{9}
R		7×10^{-6}	
ν	105	104	103
χ^2/ν	6.2	2.0	1.5

Table 3: Model parameters for the 1991 June 30 flare.

CONCLUSIONS

STOCHASTIC ACCELERATION

MODEL PARAMETERS

$5 \times 10^{10} < n < 3 \times 10^{11}\ cm^{-3}$

$300 < B < 500\ G$

$L \gtrsim 10^{9}\ cm$

TURBULENCE ENERGY $W_T \sim 10^{-5}(B^2/8\pi)$

HESSI

COMBINED HIGH SPECTRAL AND SPATIAL RESOL.

RADIO OBSERVATIONS

IMPROVED MODELS

1. OBSERVATIONS

TOTAL SAMPLE

YOHKOH Flares from Oct. '91 to Aug. '98
From "The YOHKOH HXT Image Catalog"
(Sato et al. 1998)

LIMB FLARE SAMPLE (Masuda's selection criterion)

Heliocentric longitude > 80 degrees
Channel M2 Flux ≥ 10 counts/sec/SC

IMAGES AND LIGHT CURVES

SPECTRAL INDICES

LOOPTOP vs FOOTPOINT EMISSION
CHARACTERISTICS

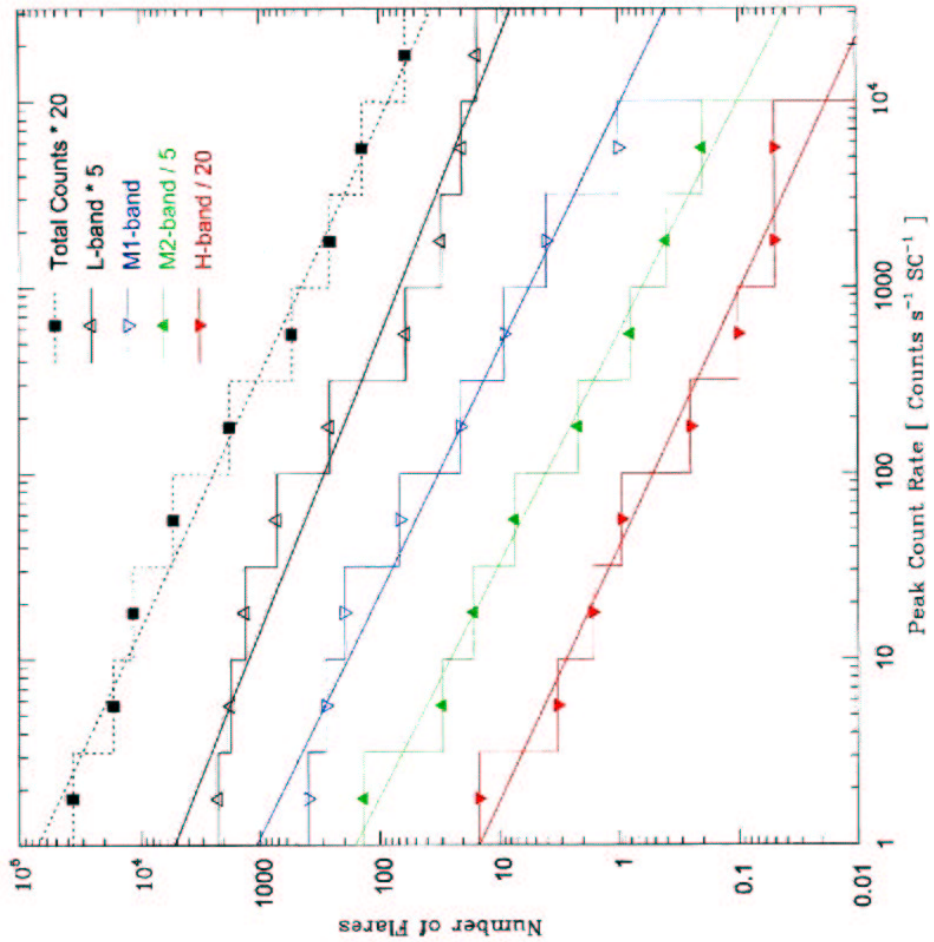

Event #	Date	Peak Time hhmmss	Disk Position	GOES Class	L band Peak Count	Loop Top Location
1	91/12/02	045527	N18E84	M3.6	61	inside*
2	91/12/15	024411	——	M1.2	30	NO SXT
3	91/12/18	102740	S14E84	M3.5	379	inside(New)
4	92/01/13	172937	S16W84	M2.0	51	above*
5	92/02/06	032511	N06W84	M7.6	807	inside(s-hot)
6	92/02/17	154209	N16W80	M1.9	33	inside
7	92/04/01	101407	——	M2.3	50	no LT source*
8	92/10/04	222107	S05W90	M2.4	35	above
9	92/11/02	030002	S24W84	X9.0	11608	Int.
10	92/11/05	061959	S18W84	M2.0	68	none
11	92/11/23	202602	S08W84	M4.4	94	NO SXT
12	93/02/17	103630	S07W87	M5.8	229	above
13	93/09/27	120839	N08E84	M1.8	70	above
14	93/11/30	060337	S20E84	C9.2	57	C
15	98/04/23	054454	S20E84	X1.2	1496	single*
16	98/05/08	015847	S16W84	M3.1	116	C
17	98/05/09	032641	S16W84	M7.7	860	NO SXT
18	98/05/10	131849	S28E84	M3.9	138	Int.
19	98/08/18	082141	N34E84	X2.8	3499	inside?
20	98/08/18	221534	N30E84	—-	12397	C

Table 1: List of events from October 1991 to August 1998 that satisfy Masuda's two criteria. Dates, UT times, position on the solar disk, flare classifications and the Peak Counts in the L band (columns 2 to 6) are taken from Sato et al. (1998). Column 7 describes the location of the LT HXT source relative to the SXT loop and some other characteristics of the images. The horizontal line divides the Masuda (pre September 1993) flares and our post September 1993 flares. Flares identified by a * may be partially occulted by the solar limb. NO SXT implies absence of SXT image of the loop. Flare # 3 labeled (New) was missed by Masuda. Flare # 4 was classified by Masuda as a super-hot thermal source. Flare # 15 (identified as single*) shows presence of only one resolved source which may be the LT source of an occulted loop. C=complex multiple loop event. Int.= Interrupted observation, not analyzed.

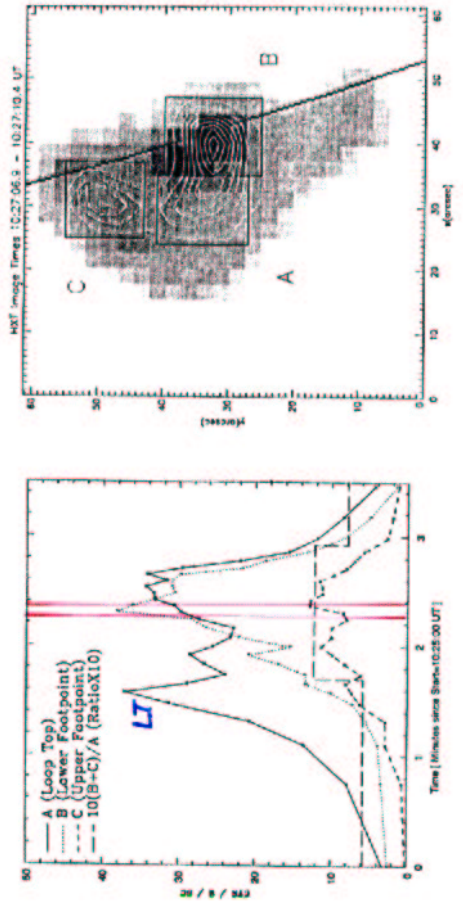

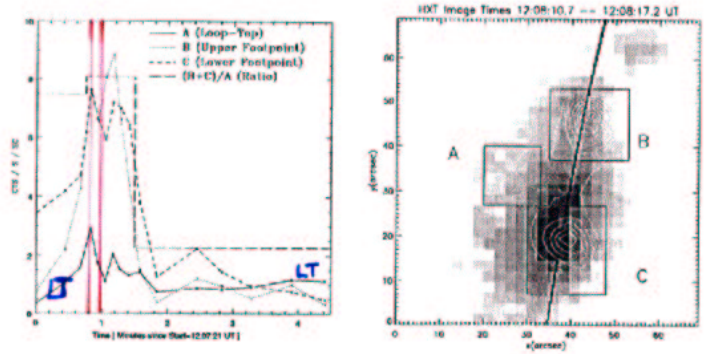

Fig. 2.— Same as Figure 1 for the September 27, 1993 flare, with $B_{max} = 4.1$ and $\Delta B = 0.41$ counts/pixel.

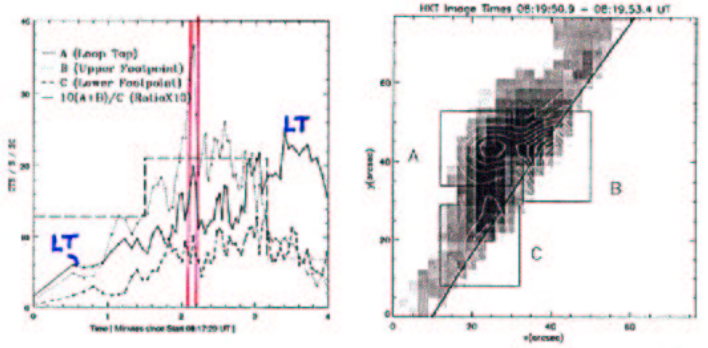

Fig. 3.— Same as Figure 1 for the first August 18, 1998 flare, with $B_{max} = 1.9$ and $\Delta B = 0.15$ counts/pixel.

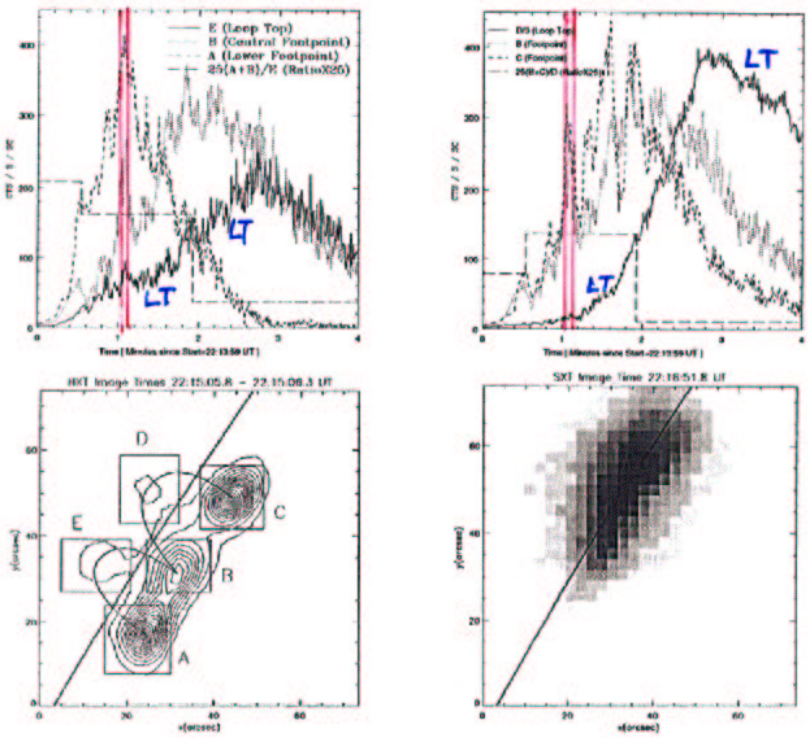

Fig. 4.— Same as Figure 1 for the second August 18, 1998 flare. The upper left and right panel light curves represent the southern (AEB) and the northern (BDE) loops, respectively. Note that for the LT source D we plot counts divided by 3. In the HXT image (lower left panel) $B_{max} = 14.8$, $\Delta B = 0.82$ counts/pixel, the digonal line shows the limb location, and the two arcs sketch the presumed loop outlines. The SXT image is shown separately on the lower right panel to avoid confusion. Note that the SXT image was taken nearly two minutes after the HXT image, which could explain the slight misalignment between the two images.

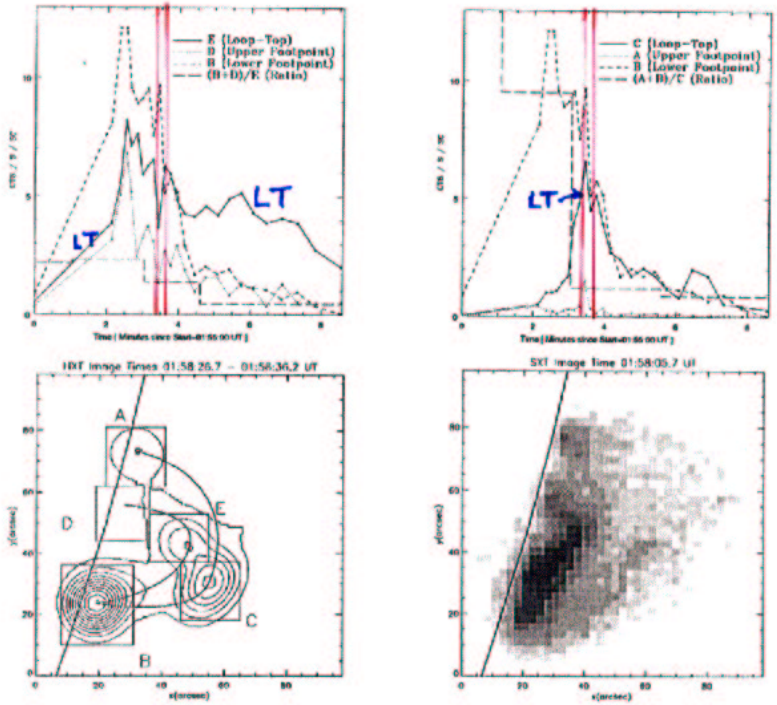

Fig. 5.— Same as Figure 4 for the May 8, 1998 flare. The upper left and right panel light curves represent the inner (DED) and the outer (ACB) loops, respectively. In the HXT image $B_{max} = 3.0$ and $\Delta B = 0.23$ counts/pixel. These images were reconstructed using the "pixon" method.

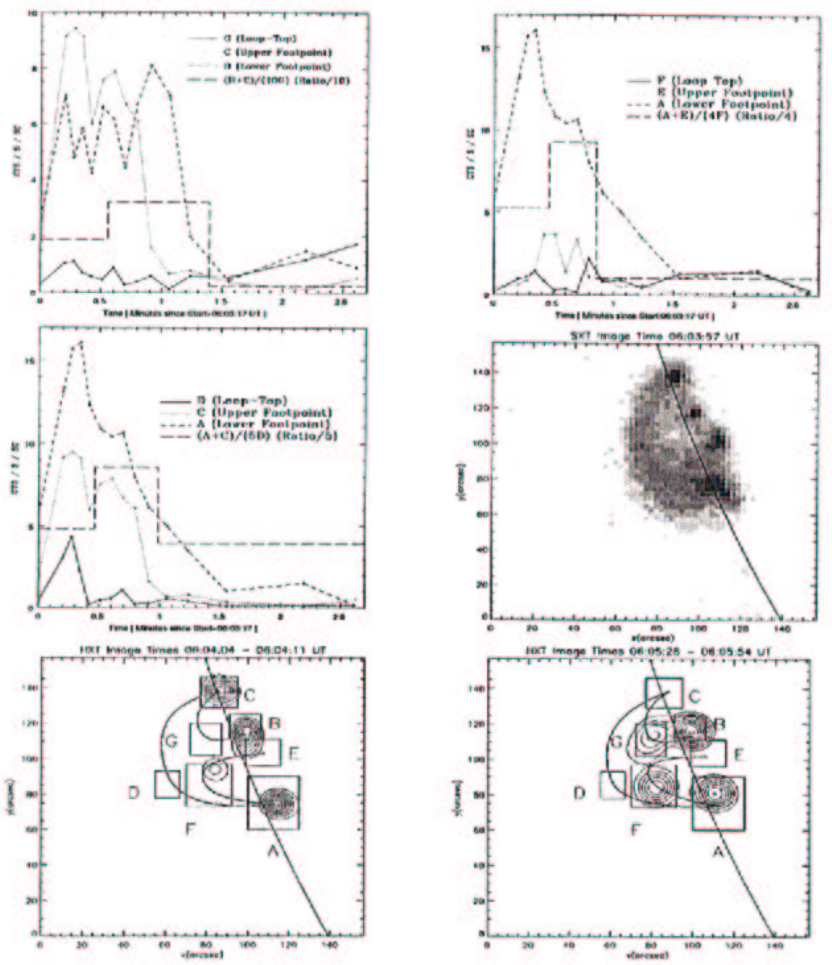

Fig. 6.— Same as Figure 4 for the November 30, 1993 flare. The light curves in the middle left panel represents what may be the outer flaring loop (ADC), while those in the upper two panels represent other sources seen in the flare, which may form two inner loops (CGB and EFA). The SXT image is shown in middle right separately and two HXT images at two different times are shown at the lower panels, with $B_{max} = 2.5$ and $\Delta B = 0.23$ counts/pixel for the left panel, and $B_{max} = 1.7$ and $\Delta B = 0.16$ counts/pixel for the right panel. These images were reconstructed using the "pixon" method.

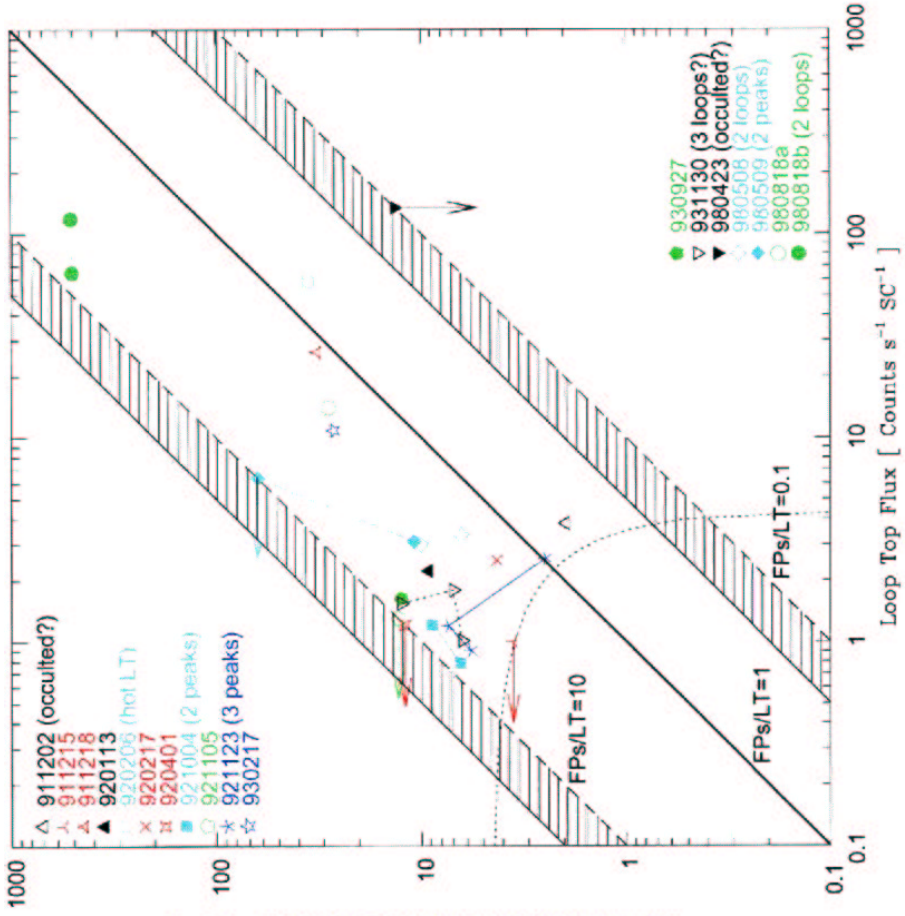

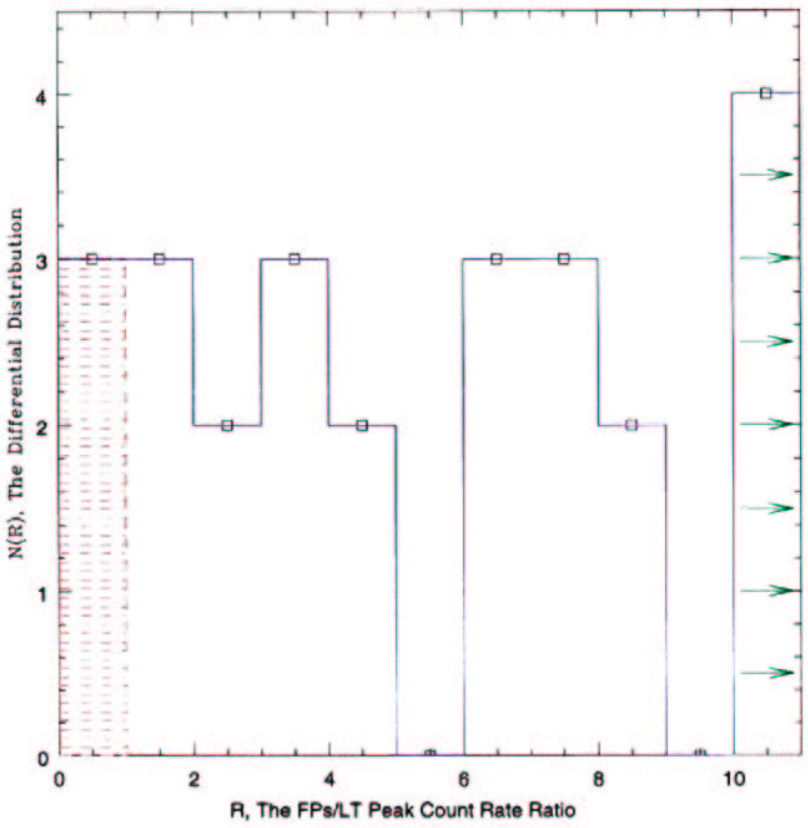
N(R), The Differential Distribution
R, The FPs/LT Peak Count Rate Ratio
0
1
2
3
4
0
2
4
6
8
10

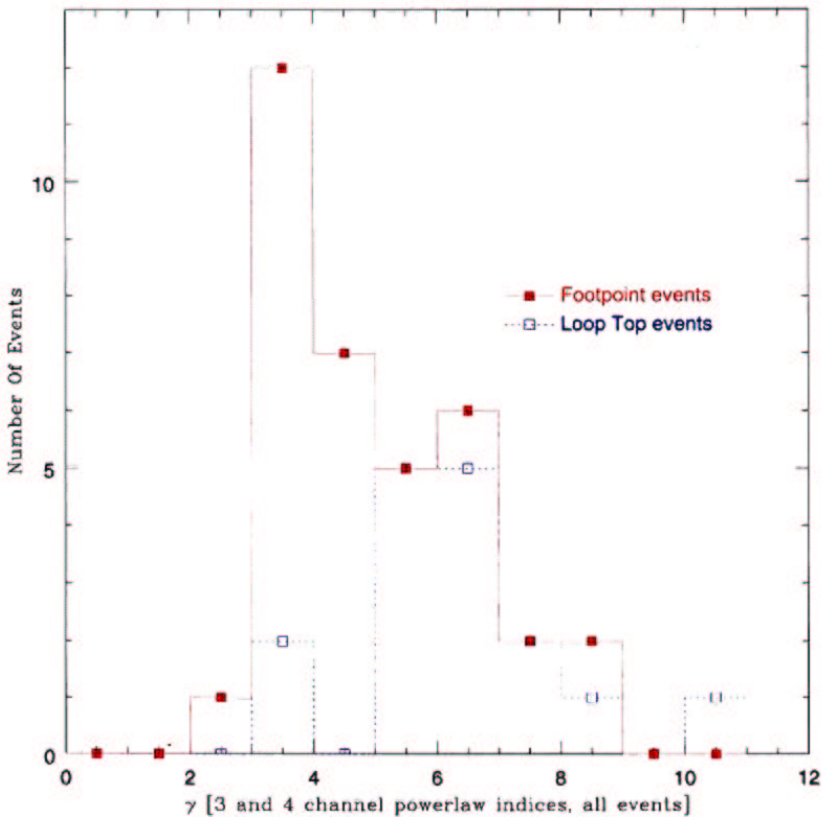
Number Of Events
γ [3 and 4 channel powerlaw indices, all events]
Footpoint events
Loop Top events
0
5
10
0
2
4
6
8
10
12

Emission Ratio vs. $D T_{esc}$

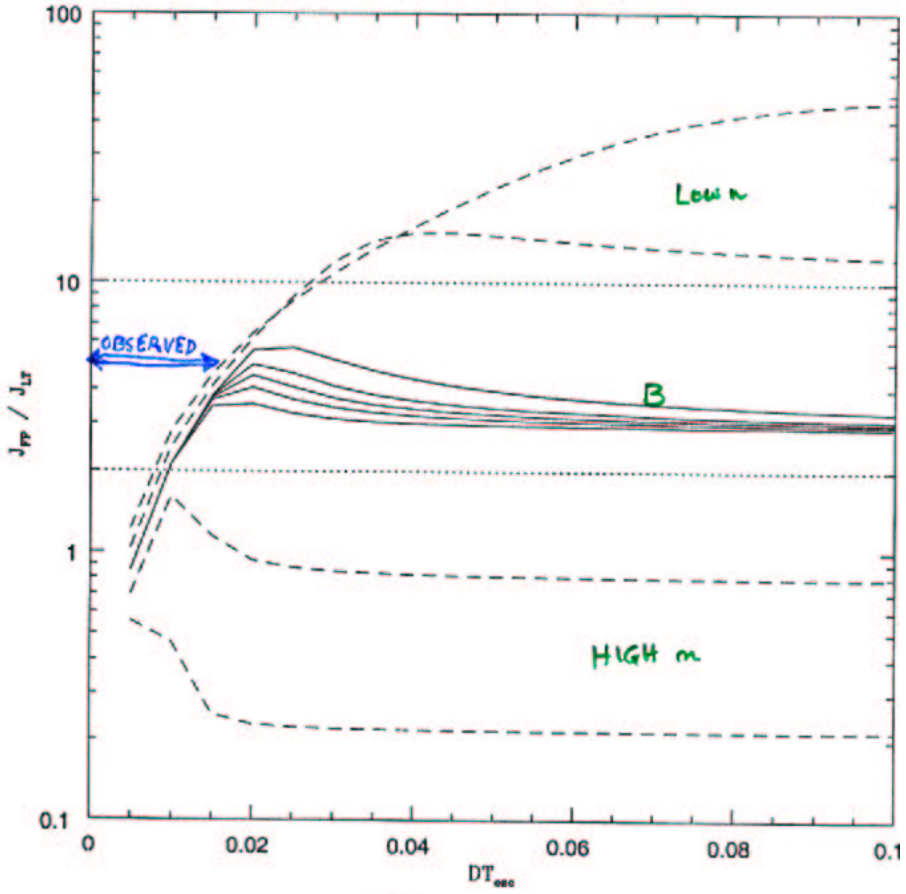

$D T_{esc}$

Spectral Index vs. $D T_{esc}$

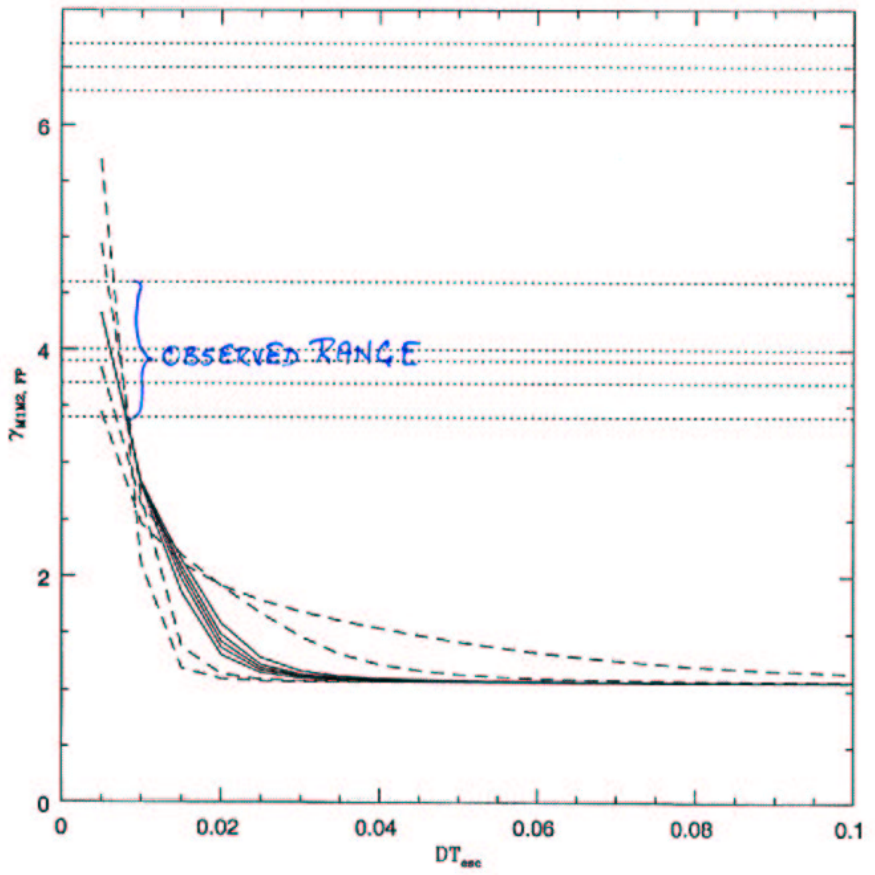

γ

$D T_{esc}$